Hydrogeological model of the Baltic Artesian Basin

Janis Virbulis, Uldis Bethers, Tomas Saks, Juris Sennikovs & Andrejs Timuhins

Hydrogeology Journal
Official Journal of the International Association of Hydrogeologists

ISSN 1431-2174
Volume 21
Number 4

Hydrogeol J (2013) 21:845-862
DOI 10.1007/s10040-013-0970-7

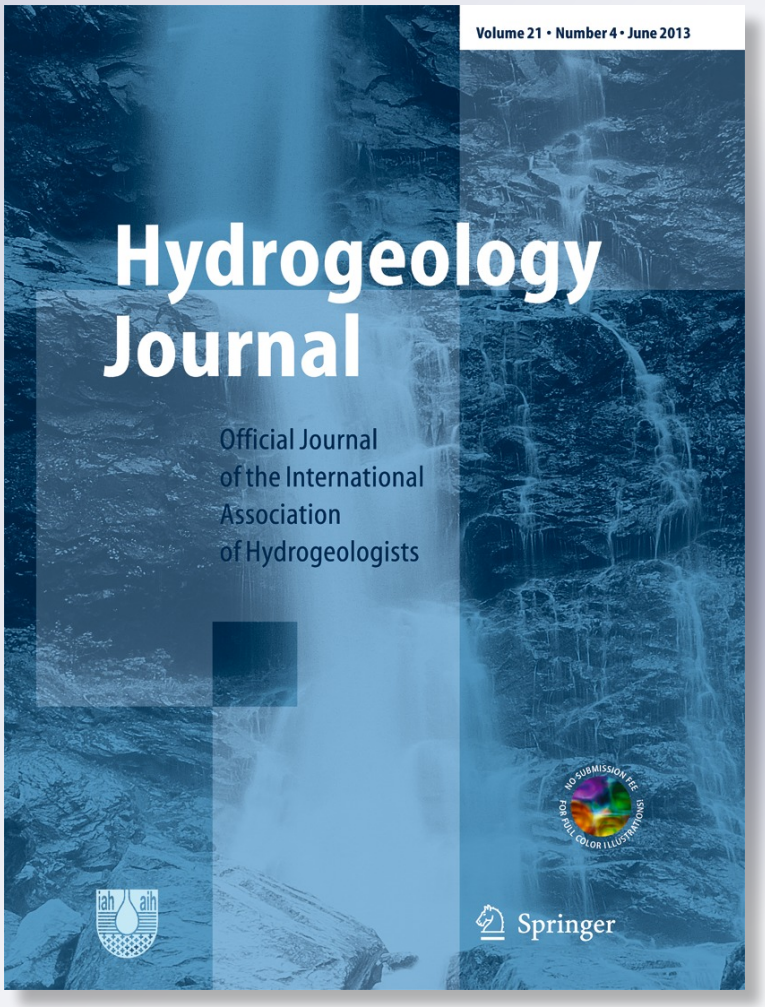

Springer

Hydrogeological model of the Baltic Artesian Basin

Janis Virbulis · Uldis Bethers · Tomas Saks · Juris Sennikovs · Andrejs Timuhins

Abstract The Baltic Artesian Basin (BAB) is a complex multi-layered hydrogeological system in the south-eastern Baltic covering about 480,000km^2. The aim of this study is to develop a closed hydrogeological mathematical model for the BAB. Heterogeneous geological data from different sources were used to build the geometry of the model, i.e. geological maps and stratigraphic information from around 20,000 boreholes. The finite element method was used for the calculation of the steady-state three-dimensional (3D) flow of unconfined groundwater. The 24-layer model was divided into about 1,000,000 finite elements. A simple recharge model was applied to describe the rate of infiltration, and the discharge was set at the water-supply wells. Variable hydraulic conductivities were used for the upper (Quaternary) deposits, while constant hydraulic conductivity values were assumed for the deeper layers. The model was calibrated on the statistically weighted borehole water-level measurements, applying L-BFGS-B (automatic parameter optimization method) for the hydraulic conductivities of each layer. The principal flows inside the BAB and the integral flow parameters were analyzed. The modeling results suggest that deeper aquifers are characterized by strong southeast–northwest groundwater flow, which is altered by the local topography in the upper, active water-exchange aquifers.

Keywords Baltic Artesian Basin · Groundwater flow · Numerical modeling · Inverse modeling

Received: 8 February 2012 / Accepted: 24 February 2013
Published online: 26 March 2013

J. Virbulis (✉) · U. Bethers · T. Saks · J. Sennikovs · A. Timuhins
University of Latvia,
Raina blvd. 19, 1586 Riga, Latvia
e-mail: janis@modlab.lv
Tel.: +371-29148600
Fax: +371-67033781

Introduction

Groundwater is the main source of drinking water in the Baltic States, and is also a major source of water for industry and agriculture. Despite the huge groundwater resources, sustainable use of large water-extraction operations over large regions is only possible by considering the response of the groundwater system to human-induced forcing, i.e. considerable reduction of the groundwater level or intrusion of salt water in coastal regions. The comprehensive basin approach allows one to correctly assess the results of both short- and long-term effects of interventions in the aquifers, and to carry out risk assessments associated with such actions, e.g. plans for CO_2 storage in the deep aquifers, aquifer-vulnerability management, etc. There is a potential for the use of geothermal energy in the deepest aquifers (Normani and Sykes, 2012).

Previous modeling studies in the territory of the Baltic Artesian Basin (BAB) consist of smaller-scale models in different countries. There are several local modeling studies of the groundwater flow in Poland, Estonia, Latvia and Lithuania. The distribution of groundwater heads in the territory of Estonia and surrounding coastal areas were modeled using Visual MODFLOW by Vallner (2003). The groundwater flow is modeled in an area of 26,000 km^2 including nine aquifers in the central part of Latvia, the northern part of Lithuania and a large part of the Gulf of Riga by Spalvins et al. (1996). The reconstruction of the hydrogeological conditions during the late Pleistocene and Holocene has been performed for the southern part of the BAB situated on the slope of the Belarusian-Masurian crystalline basement using the finite element (FE) model FEFLOW by Zuzevicius (2010). The regional hydrogeological model for the south-east of Lithuania is based on Groundwater Vistas software (Spalvins et al. 2009). The formation of groundwater runoff in the Nemunas River Basin including shallow groundwater, surface water and underlying confined aquifers has been modeled using MODFLOW 2005 (Stuopis et al. 2010). The three-dimensional (3D) geological model of Poland is one of the first country-wide

 DOI 10.1007/s10040-013-0970-7

models including an area of 312,000 km^2 with a horizontal resolution of 500 m; however, the groundwater flow has not been modeled (Malolepszy 2005).

There are several other examples of regional models of artesian basins. The history of groundwater modeling in the Great Artesian Basin in Australia is described by Welsh and Doherty (2005). The transient groundwater model of the Great Artesian Basin in Australia runs under MODFLOW-2000 with a 5 × 5-km grid cell size, more than 60,000 active cells and only one vertical layer (Welsh 2006). In the West Siberian Artesian Basin, the CFEST code is used to model the steady-state groundwater flow in five layers (Foley 1994). Although all possible data sources were used, the rough mesh cannot feasibly include topological and hydrological information for a 3.5-million-km^2 area of basin. The groundwater flow in the Bengal Basin (India and Bangladesh) was modeled using MODFLOW with 7 vertical units (34 model layers) and 328,461 active cells, the size of the grid cell being 5 km (Michael and Voss 2009).

However, none of the modeling studies in the Baltic region deal with the BAB as a closed system, primarily because of poor coverage or lack of data in the Baltic Sea, or hard accessibility of data in the neighboring countries leading to geometrical model borders coinciding with political borders of the particular country. Such an approach leads to implausible boundary condition solutions on the borders of the model, as the pressure head or groundwater flow velocity data are often very general and sparse. On the other hand, building a model for the whole sedimentary basin, and treating it as a closed system, allows one to avoid these uncertainties; however, the uncertainties of the geological structure in the poorly explored regions of the basin such as the Baltic Sea area, can become an issue.

Different methods are used in the modeling of the groundwater flow. The de facto standard application in groundwater modeling is MODFLOW (McDonald and Harbaugh 1989), based on a finite difference method. FEFLOW is a commonly used FE software for simulating density coupled flow, and mass and heat transport in the subsurface (Trefry and Muffels 2007). Even the cellular automata method is used in the modeling of the two-dimensional (2D) water flow in unconfined aquifers (Ravazzani et al. 2011).

Modelers of groundwater flow have to deal with conceptual model uncertainty (notably, spatial and temporal variability), scale dependence and many types of unknown parameters such as hydraulic conductivity, recharge, boundary conditions, etc. (Carrera et al. 2005). The calibration of the model is part of the model development.

The objectives of this work are (1) to build the geometric structure of the whole BAB as a FE mesh, (2) to develop the model and software for steady-state groundwater flow calculation, (3) to calibrate the model based on the observed water levels in boreholes, and (4) to calculate the principal flows and integral characteristics of the BAB. The model will be used as a basis for further developments in modeling the age of the groundwater, the formation of its chemical composition, the processes involved in glacial water intrusion and others. The model is also intended as a platform for the modeling of local problems on a smaller scale and/or with a higher data density level inside the BAB.

Geology and hydrogeology of the BAB

The BAB is a multi-layered sedimentary basin and a complex hydrogeological system underlying about 480,000 km^2 in the western part of the East European Platform. The BAB includes the territory of Latvia, Lithuania and Estonia and parts of Poland, Russia and Belarus but approximately half of the BAB is covered by the Baltic Sea. The thickness of the sedimentary cover reaches 5,000 m in the south-western part, while the crystalline basement reaches the surface at the northern and south-eastern parts of the study area. The Eidiacaran (Vendian) Complex and Cambrian sediments are the oldest sedimentary rocks, while the Quaternary deposits lie at the top and are comprised mostly of glacial sediments.

From the hydrogeological point of view, the BAB consists of aquifers and aquitards of different spatial distribution and thicknesses. The crystalline basement, at the bottom, is treated as an impermeable aquitard. The aquifers are mostly confined, and only a part of the Quaternary layer is partially unconfined. The slightly conductive aquitards in the zone of the active water exchange do not ensure a complete isolation of aquifers, thus the conditions of vertical water exchange between aquifers are rather favorable (Juodkazis and Paltanavicitjs 1976).

The study area is a part of the East European Platform. Cambrian to Silurian deposits constitute the Caledonian sequence. The surface elevation of this sequence generally follows the structure of the crystalline basement (Brangulis and Kaņevs 2002), is quite intensely faulted, and the sequence geometry is mainly controlled by the amount of displacement along the faults and the rate of erosion during Late Silurian–Early Devonian period (Brangulis and Kaņevs 2002). The Cambrian is predominantly composed of marine sandstones, siltstones and clays and these form the lower aquifer system in the BAB (Brangulis, 1985). The Ordovician and Silurian sequences are composed of the deeper marine facies—marine clays, limestones and marls, and the whole sequence, except the most upper Silurian layer in northern Estonia, is treated as an aquitard in the present study. Sediments of an overlying Herzynian sequence (Devonian up to Permian) are less deformed with less pronounced fault activity. The Lower Devonian sequence discordantly overlies the Caledonian sequence rocks. It consists mainly of sandstone beds and, in this study, the whole sequence is treated as an aquifer.

The Middle Devonian Narva formation is composed mainly of clays, siltstones and marls, and is treated as an aquitard in this study. It covers most of the central part of the BAB and therefore forms a regional aquitard, separating the slow water exchange zone beneath it from

 DOI 10.1007/s10040-013-0970-7

the active water exchange zone above it. The Middle and Upper Devonian formations, mainly composed of sandstones, cover the Narva formation. This sandstone sequence is divided into two aquifers, separated by a thin aquitard. The rest of the Upper Devonian is subdivided into two aquifers and one aquitard, depending on the predominant composition. The Carboniferous, Permian and Mesozoic sediments in the mainland area cover a relatively small area, but their thickness increases towards the SW corner of the BAB, where the thickness of this sequence increases up to 3 km.

The sedimentary basin considered has been considerably faulted, with the greatest displacements occurring along the Pleskava (Pskov)–Liepāja fault zone (Brangulis and Kaņevs 2002). The faulting activity is present in the deepest part of the basin, and generally the faulted rocks of the Caledonian age are covered by the relatively unfaulted Lower and Middle Devonian sediments. However, faults are a very important factor regarding the aquifer connectivity for the Cambrian aquifer system. It can be seen that half of this aquifer system is disconnected by faults along the Pleskava (Pskov)–Liepāja fault zone, which has an effect on the groundwater flow in this aquifer system. Secondly, it has been shown (Folch and Mas-Pla 2008; Cherubini and Pastore (2011) that faults themselves can serve as planar, nearly vertical aquifers and connect the otherwise disconnected aquifers along the strike of the faults. However, intrinsic fault properties were not considered, as it is beyond the scope of the current study.

Data sources

There are many sources of data on the geological structure of the BAB. However, the heterogeneous nature of the data posed a challenge in its unification in order to be used as an input in the geometrical structure of the model. The information sources include:

1. Structural maps of the topography of several formations for Latvia (4 maps) and Lithuania (13 maps from the database of the State Geological Survey of Lithuania; Brangulis et al. 1998)
2. Geological maps of the sub-Quaternary for Latvia and Lithuania
3. Structural maps of the crystalline basement in Latvia and the BAB—Brangulis et al. (1998); Vetrennikovs (1996)
4. Data for around 20,000 boreholes in the territory of Latvia from the database of the Latvian Environment, Geology and Meteorology Center (LEGMC; Takčidi 1999)
5. Geological model of Estonia by Vallner (2003)
6. Surface topography from Shuttle Radar Topography Mission (SRTM) data with 25-m resolution (Jarvis et al. 2008)
7. Bathymetry of the Baltic Sea (Seifert et al. 2001)
8. Data from published geological cross-sections
9. Literature studies: Vetrennikovs (1996); Sorokin et al. (1981); Kovalevskij and Ozolins (1967); Brangulis (1985); Ulste (1961) and Tuulig and Floden (2009)
10. Hydrogeological atlas of Poland (Paczynski et al. 1993)
11. Hydrogeological maps of the Baltics, 1:500000 (Juodkazis 1982)
12. The geology of the southeastern Baltic Sea (Usaityte 2000)

Groundwater abstraction data in Latvia, Lithuania and Estonia were used to set up the sources of water abstraction. Observations of piezometric heads in the monitoring wells were used for the calibration of the model. These data were supplied by LEGMC, Geological Survey of Lithuania and Geological Survey of Estonia.

Geometric model

The FE method was employed for the calculation of the 3D flow of unconfined groundwater, as described in the next section and FEs were used for the building of the geometric structure of the model. The significant advantages of the FE method compared to the finite difference method is the more accurate representation of layering and internal boundaries (rivers, faults, edges of layers etc.) as well as the possibility of refinement of the local mesh.

The 3D mesh was constructed layer-wise. The triangular mesh in the horizontal plane was constructed so that it incorporated characteristic lines such as rivers, coastlines, borders of countries and areas of the distribution of geological layers. The boreholes later used for calibration were also included in the mesh as nodes. Additionally, fault lines were also taken into account—the 2D mesh was cut along the fault lines and the nodes were duplicated along them. The target area of triangles is non-uniform, starting from 10 km^2 in areas with dense geological information (Baltic States) up to 100 km^2 in the area of the Baltic Sea. The side length of the triangles is even smaller near the lines and points included in the mesh. The top view of the surface mesh is shown in Fig. 1.

The model of the geological structure consists of 24 layers including aquifers and aquitards from Cambrian up to Quaternary deposits (see legend in Fig. 2 for the list of layers and Table 1). The symbol $*$ was used for those aquitards that have the same stratigraphic unit name as an aquifer, disregarding the rank of the stratigraphic units. In all, 25 surfaces of the geological layers were constructed on the 2D mesh from available data sources.

Generally, the information about the layer topography or thickness, available in discrete points (boreholes, maps, or published vertical cross-sections) was interpolated or extrapolated on the triangular 2D mesh. A typical procedure was as follows: first, a set of points describing the position of a geological surface was created from boreholes and/or isolines of a geological surface; next, the 2D triangulation mesh was created from these data points

 DOI 10.1007/s10040-013-0970-7

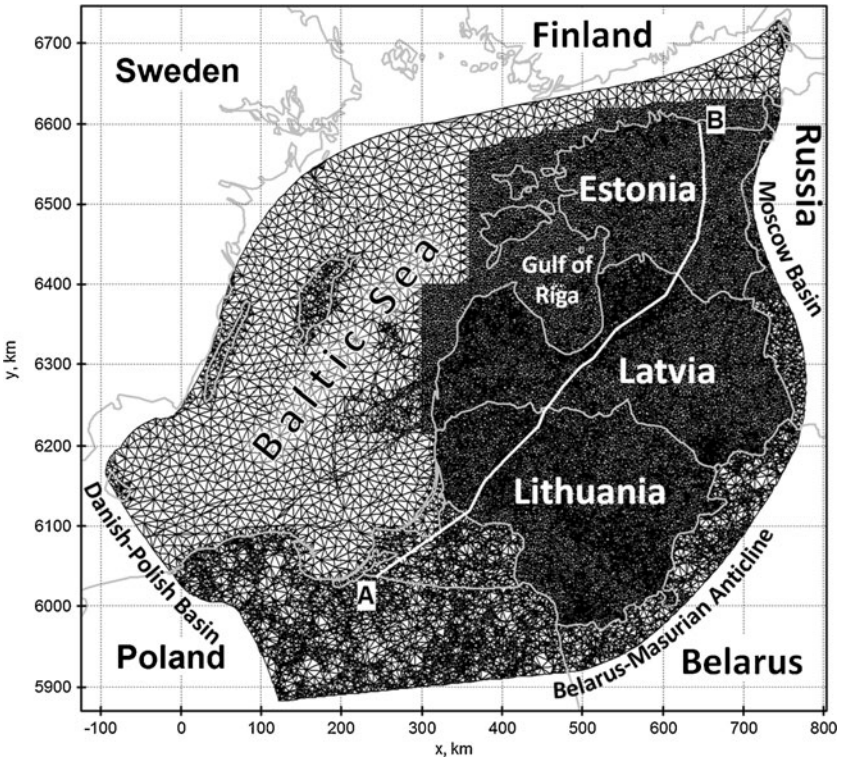

Fig. 1 Triangular 2D base mesh of the Baltic Artesian Basin. *Grey lines*: borders of the countries. *White line*: cross-section AB

and the topography from this mesh was interpolated on the base mesh of the geological structure. After that the smoothing function was applied and the values were extrapolated to empty areas within an area of the layer considered. If several sets of data were created for the same surface (e.g. in Latvia from boreholes and in the whole BAB from isoline maps), then the values from different areas were combined with a given priority. Smoothing of the surface could be repeated after every step.

The smoothing is not effective across the fault lines due to cuts in the mesh and, therefore, distinct vertical displacements along the fault lines are present. If the layer's upper surface was built using layer thicknesses (which are often smoother than the layer surface due to the inaccurate reference of the borehole position), the previously described algorithm was used for the layer thickness (instead of the z-coordinate) and these data were added to the position of the deeper surface.

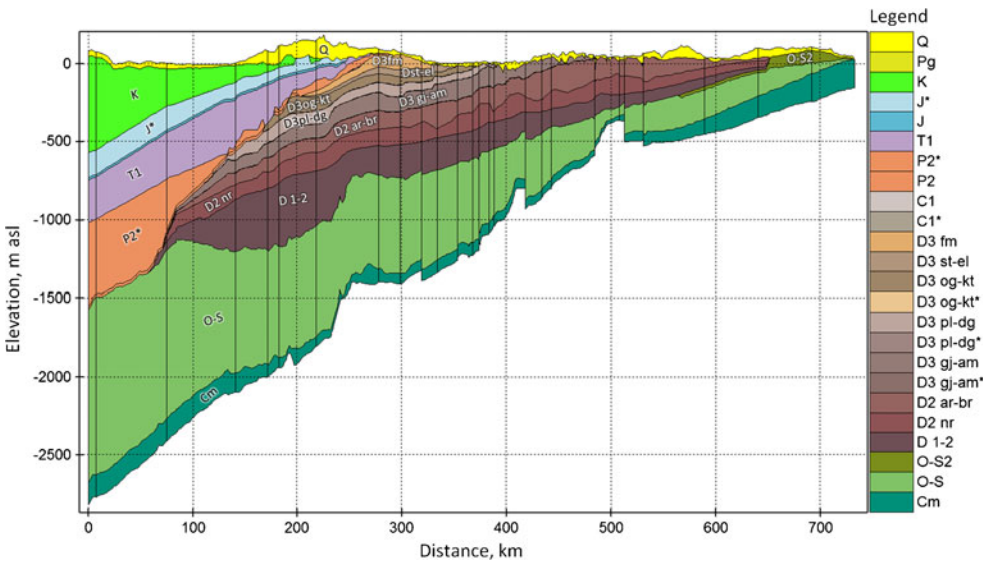

Fig. 2 The cross-section of the BAB along the line AB (see Fig. 1 for the cross-section line position). *Black vertical lines* show the faults

 DOI 10.1007/s10040-013-0970-7

Table 1 Initial and optimized values of hydraulic conductivities [K, m/day] for stages 1 and 2, the significance of the parameter (p-value) and derivative of the relative target function (Z_K)

Geological unit	Layer	Initial K		Optimized K		p-value	Z_K
		Stage 1	Stage 2	Stage 1	Stage 2		
Paleogene and Neogene	Pg	10.00	2.25	9.13	2.23	0.042	0.0000
Cretaceous	K	2.00	3.19	0.32	4.21	<0.001	0.0038
Middle–Upper Jurassic from Middle Callovian Substage to Tithonian stage formations	J*[a]	1.0E-05	6.5E-05	6.0E-05	4.7E-05	<0.001	0.0094
Lower–Middle Jurassic, Lower Callovian Substage formations	J	10.00	0.16	3.06	0.22	<0.001	−0.0103
Lower Triassic Induan and Olenekian stages	T1	1.0E-06	5.7E-07	1.0E-05	7.7E-07	<0.001	−0.0069
Former Upper Permian, former Kazanian and Tatarian Stage Prieglius, Žalgiriai, Aistmares, Galindai, and Mamonovo formations	P2*[a]	1.0E-05	8.7E-05	1.0E-04	7.6E-05	<0.001	−0.0263
Former Upper Permian, former Kazanian stage Kalvaria, Sasnava, and Naujoji Akmene formations	P2	2.00	3.07	3.74	2.39	<0.001	0.0005
Carboniferous, Lower Mississippian, Tournaisian stage Nica formation	C1	2.00	1.89	1.98	1.42	<0.001	0.0014
Carboniferous, Lower Mississippian, Tournaisian stage Letiza and Paplaka formations	C1*[a]	1.0E-04	5.8E-04	1.6E-05	7.9E-04	0.018	−0.0005
Upper Devonian Famennian stage, Joniskis, Kursa, Akmene, Muri, Tervete, Snikere, Zagere, Ketleri and Skervelis formations	D3fm	2.00	0.49	0.23	0.37	0.049	−0.0056
Upper Devonian Frasnian and Famennian stage Stipinai, Amula and Eleja formations	D3st-el	1.0E-04	9.7E-06	1.9E-05	7.2E-06	<0.001	−0.0037
Upper Devonian Frasnian stage Ogre formation	D3og-kt	1.00	0.19	0.27	0.25	<0.001	0.0004
Upper Devonian Frasnian stage Katlesi formation	D3og-kt*[a]	1.0E-05	6.3E-08	1.0E-06	4.3E-08	0.203	0.0006
Upper Devonian Frasnian stage Pļaviņas, Salaspils and Daugava formations	D3pl-dg	10.00	2.26	2.75	1.69	<0.001	0.0529
Upper Devonian Frasnian stage lower part of the Pļavinas formation	D3pl-dg*[a]	1.0E-07	8.8E-07	1.5E-07	6.4E-07	0.190	0.0342
Upper Devonian Givetian–Frasnian stage Gauja–Amata formations	D3gj-am	2.00	2.04	5.94	2.91	<0.001	0.0258
Upper Devonian Givetian stage upper part of the Burtnieki formation	D3gj-am*[a]	2.0E-07	2.7E-05	6.9E-07	3.7E-05	<0.001	−0.0075
Middle Devonian Eifelian stage Arukula formation and Middle Devonian Givetian stage Burtnieki formation	D2ar-br	2.00	0.40	0.27	0.55	<0.001	0.0066
Middle Devonian Eifelian stage Narva formation	D2nr	1.0E-06	2.3E-09	3.2E-06	2.1E-09	<0.001	0.0000
Lower–Middle Devonian formations (Tilze, Stoniskiai, Kemeri, Rezekne, Pernava formations)	D1-2	2.00	2.31	1.84	1.62	<0.001	0.0220
Upper Ordovician–Upper Silurian Pridolian series	O-S2	2.00	1.11	0.27	1.49	<0.001	0.0038
Silurian–Ordovician	O-S	1.0E-09	1.0E-09	1.1E-09	1.1E-09	<0.001	0.0000
Ediacaran (Vendian)–Cambrian	Cm	1.00	3.63	0.55	2.95	<0.001	−0.0435

[a] An aquitard that has the same stratigraphic unit name as an aquifer, disregarding the rank of the stratigraphic units

Several thin conceptual Devonian aquitards (D3pl-dg*, D3gj-am*, D3og-kt*) with a constant thickness of 2 m and the Permian aquifer P2 (thickness 20 m) and Jurassic aquifer J (thickness 30 m) were added. The next step was building the 3D mesh from the set of surfaces. First, the surface of the crystalline basement was set as the bottom surface of the mesh. Next, the Cambrian (Cm) surface was added and the volume elements for the Cm layer were created between the basement and the Cm surface. The surfaces (as absolute position or difference from the previous surface) were continuously added on top of each other. It can turn out that the layer surface topography is inconsistent, i.e. the height of the lower sediment layer can be higher than that of the upper one; therefore, the positions of the surfaces had to be corrected before building the volume elements. If the extent of the layer did not cover the whole area of the BAB, wedge-shaped volume elements were formed along the boundary line and volume elements were not formed outside the boundary. This way the number of elements was reduced.

Most of the 3D FE were triangular prisms. Pyramids and tetrahedra were used near the fault lines and boundaries of geological layers, if necessary. The current version of the mesh consists of 584,000 points and 1.06 million volume elements. The building of the mesh as well as the following setup of the boundary conditions, calculation and calibration was realized as a Python language script which can be run either in a Windows or Linux environment. The script invoked stand-alone executables for particular time-consuming procedures as solvers etc. The main advantage of the developed script system is the reproducibility of the geometric structure. All algorithms and data sources used during the building of the structure are documented in the script. The cross

 DOI 10.1007/s10040-013-0970-7

section along the line AB in Fig. 2 illustrates the geological structure of the BAB.

Hydrogeological model

The governing equation of steady-state 3D Darcy flow with anisotropic conductivity is:

$$\frac{\partial}{\partial x}\left(K_{xy}\frac{\partial h}{\partial x}\right)+\frac{\partial}{\partial y}\left(K_{xy}\frac{\partial h}{\partial y}\right)+\frac{\partial}{\partial z}\left(K_{z}\frac{\partial h}{\partial z}\right)+q=0, \quad (1)$$

where h is the piezometric head, q is the volume of abstracted water, and K_{xy} and K_z are the horizontal and vertical hydraulic conductivities, respectively.

The position of the water table is assumed to be the same as the calculated head h in the top layer. As all the layers excluding the Quaternary layer are confined and usually only a small part of the Quaternary layer is unconfined, the conductivities are not adapted according to the water content in an element, as is often done for unconfined aquifers (McDonald and Harbaugh 1989). This increases inaccuracy in the unconfined parts of the Quaternary layer but avoids possible numerical instabilities and saves calculation time since no additional iterations for hydraulic conductivities K are necessary.

The FE method with Galerkin weighted residuals is used for solving Eq. (1). Bilinear prisms and 5-point pyramids as well as linear tetrahedrons are used as FEs (Zienkiewicz and Taylor 2000). The integration of elements is performed numerically using the second order Gauss quadrature so the integrals fit the exact analytical solution for linear elements with constant material properties. The conductivities are assumed to be constant inside the FEs.

The FE method results in an algebraic equation system. During the formation of its global FE matrix only non-zero elements and a connection matrix are created. The system is solved using the direct sparse solver PARDISO (Schenk and Gartner 2006).

Boundary conditions

The Precambrian basement forms the impermeable bottom of the model as suggested by Levins et al. (1998) and Mokrik (1997). On the northern and western side of the BAB the basement reaches the earth surface and the thickness of the model is zero. On the southwestern side, the BAB borders the Danish-Polish Basin with a zone of extensive faulting and this boundary is assumed to be impermeable (according to Mokrik 1997). The eastern side of the BAB is connected with the Moscow Artesian Basin and the south-eastern boundary is the Belarus-Masurian Anticline. The thickness of the BAB at these boundaries is approximately 300–500 m. Zero water exchange is assumed through these boundaries.

A simple recharge model is applied on the surface. The level of the lakes, rivers and the sea is fixed as a constant hydraulic head in corresponding nodes. The infiltration is set as a flux boundary condition in surface elements which contain at least one point where hydraulic head is not fixed. Most of the approximately 1,000 mm/year meteoric water is evaporated or collected in streams and rivers on a sub-mesh scale and must be excluded from the infiltration flux. The exact calculation of the infiltration flux requires an extensive hydrology model coupled with groundwater modeling which is outside the scope of the current study. Instead, a constant mean value of 70 mm/year was assumed as an infiltration flux for the whole BAB area; this value was adjusted during the automatic calibration process. However, in some areas with lower hydraulic conductivity, or in lowlands, this value can still be higher than what would be possible for water to infiltrate, and the soil is saturated and

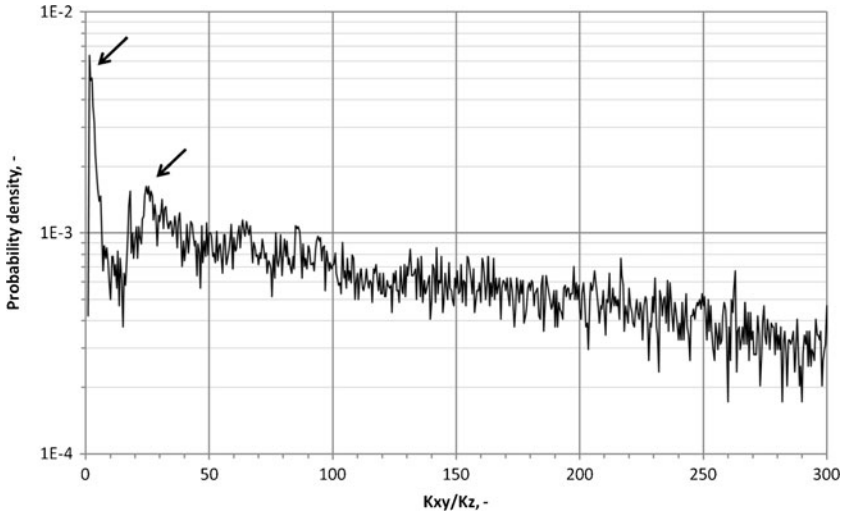

Fig. 3 Probability density distribution of ratio K_{xy}/K_z in Quaternary deposits in Latvia

 DOI 10.1007/s10040-013-0970-7

additional runoff will take place. In such a case, the calculations applying high infiltration as a flux boundary condition will result in water levels higher than the earth surface. To avoid this non-realistic result, the water level is set equal to the earth surface level, assuming that the remaining water will be transported away by surface runoff and is not included in the groundwater modelling. This is equal to the setting of a fixed head boundary condition in the calculation algorithm.

To describe this process, iterations are performed to adjust the boundary conditions in elements where the infiltration boundary condition is set. The results of the first iteration are analysed automatically and if the water level is higher than the earth surface, a fixed hydraulic head equal to the ground surface level is set at the corresponding points for the next iteration. In elements where the head is lower than the earth's surface, the same flux boundary condition as in the first iteration is applied. Only two iterations (each of them computed with the direct solver) are necessary to achieve the converged solution.

Numerically the infiltration flux is set at a constant value on the boundary face of a FE and is integrated using the second order Gauss quadratures in either triangle or quadrangle. The fixed head condition is set as a constant value in the nodes as the last step in the formation of the matrix.

Only abstraction wells with larger yields are taken into account. A total of 49 wells in Lithuania (total abstraction 45,000 m^3/day), 161 in Latvia (184,000 m^3/day) and 172 in Estonia (24,000 m^3/day) are considered. Each q [m^3/s] source was distributed inside the enclosed finite volume element corresponding to the water abstraction conditions in the year 2000. In case the well's screen is longer than one element, the source is distributed between the elements proportionally to the length of the screen. The validation of the model against solutions of analytic problems is demonstrated in the Appendix.

Model calibration using the optimization method

The calibration of the hydrogeological model is one of the most important steps during the model development. Knowledge about the parameters of the modeled system is often insufficient, especially for the large regional models, and a lack of geometric and hydraulic conductivity data is typical. Fluid flow problems in stochastic heterogeneous media involving many length scales with large variations of filtration properties make the calibration dependent on the size of the mesh.

The modified Gauss-Newton method (Harrar et al. 2003) or genetic algorithms (Bastani et al. 2010) are typically used for calibration of the groundwater flow. The optimization method L-BFGS-B is used for the calibration of the BAB model. This is a quasi-Newton optimization method well suited for a large number of parameters where the storage for the Hessian matrices is limited according to Nocedal (1980). The procedure *fmin_l_bfgs_b* implemented in the Python optimization library *scipy.optimize* by Scipy community (2011) is used for the calculations.

The model is calibrated on the available head measurements in monitoring wells and head measurements in boreholes during the installation. Data are available from the year 1913 until present (2011); however, 90 % of the boreholes were installed after 1962 (99 % after 1953) and 90 % of the monitoring well data were measured after 1972. The available data are not uniformly distributed over the covered area and there is a distinct time dependence of the water level in the aquifers intensively used for groundwater abstraction. Therefore, instead of using the root mean square error (RMSE) to estimate model performance, a weighted RMSE was used, separating weight into spatial and temporal multipliers.

A spatial weighting coefficient $c_r(I)$ was assigned to each borehole to avoid overestimation of the borehole clusters. The coefficients are:

$$c_r(I) = \left(1/\sum_{j=1}^{N} e^{-\frac{(\mathbf{r}_I-\mathbf{r}_j)^2}{\sigma^2}}\right) / \left(\frac{1}{N}\sum_{i=1}^{N}\left(1/\sum_{j=1}^{N} e^{-\frac{(\mathbf{r}_i-\mathbf{r}_j)^2}{\sigma^2}}\right)\right), \quad (2)$$

where $\mathbf{r}_i$ is the coordinate vector of the corresponding borehole, $\mathbf{r}_j$ is the coordinate vector of j-th borehole from N boreholes in a hydrogeological layer, σ is the distance of influence, I is the unique identifier of the selected borehole and $\mathbf{r}_I$ is its coordinate vector. The term in the first brackets decreases the value of the coefficient, if other points are in the vicinity. The term in second brackets scales the sum of all coefficients to the number of boreholes N.

Year t_0=2,000 was chosen as a reference for calibration of the steady-state model. To account for the whole set of measurements, a temporal weighting coefficient c_{ti} was defined as a function of the time difference (in years) between the observation time moment t_i and the reference time moment t_0:

$$c_{ti} = \frac{e^{-\frac{(t_i-t_0)^2}{2\tau^2}}}{\sum_{i=1}^{N} e^{-\frac{(t_i-t_0)^2}{2\tau^2}}}, \quad (3)$$

here τ is the time of influence. The numerator in the equation decreases the value of coefficient depending on time span to t_0; the denominator scales the sum of all coefficients to 1.

The target function Z_j of layer j is the weighted sum of the squared differences between the observed and

 DOI 10.1007/s10040-013-0970-7

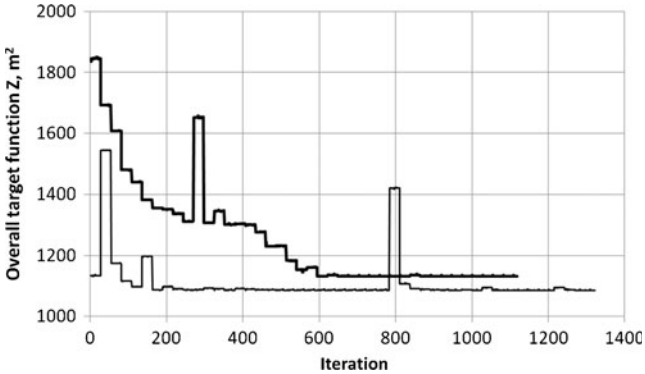

Fig. 4 Optimization procedure of the overall target function *Z*. *Bold line*, starting from parameter set 1; *thin line*, starting from parameter set 2 (see Table 1)

modeled piezometric heads:

$$Z_j = \frac{1}{\sum_{i=1}^{N} c_{ti} c_r(I_i)} \sum_{i=1}^{N} c_{ti} c_r(I_i) [h_{obs}(t_i, I_i) - h_{mod}(I_i)]^2, \quad (4)$$

here h_{obs} is the observed head, h_{mod} is the modeled head, I_I is the unique borehole identifier of the i-th observation and N is the number of the observations in the layer j. The overall target function Z, which is minimized by the optimization method L-BFGS-B, is the sum of Z_j. Equal importance of each layer is assumed and no coefficients are used in this sum:

$$Z = \sum_{j=1}^{N} Z_j, \quad (5)$$

here N is the number of layers where target function is minimized.

The water in the deep layers of Cm and O-S has high salinity and both have density up to 1.08 g/cm^3 according to Levins et al. (1998). Therefore, the observed heads in the Cm aquifer are corrected to virtual freshwater heads by multiplying the water column between the top of the O-S layer and the water level in the borehole by the density ratio measured in the corresponding borehole.

Table 2 Weighted mean error (*WME* [m]) and root mean square error (*RMSE* [m]) for layers used in calculation of the target function for *stage 1* and *stage 2*

Stratigraphic layer	WME		RMSE	
	Stage 1	Stage 2	Stage 1	Stage 2
Cm	7.7	4.1	14.8	14.2
D 1-2	0.5	−0.9	12.2	13.7
D2 nr	−4.3	−2.5	6.3	5.0
D2 ar-br	−3.6	−4.5	9.4	10.0
D3 gj-am	0.3	−1.0	10.1	9.6
D3 pl-dg	0.0	−1.0	9.0	8.4
D3 og-kt	−3.3	−4.4	10.1	8.9
D3 st-el	−4.0	−3.7	5.8	4.6
D3 fm	−4.9	−5.4	9.5	9.3
C1	−1.3	−1.7	6.7	6.3
P2	−1.3	−1.4	8.4	8.9
T1	−5.9	−4.9	6.2	5.2
J	−0.6	−1.0	4.0	4.1
Q	0.6	−0.7	7.7	7.7

The calibration parameters are the horizontal and vertical hydraulic conductivities of the hydrogeological layers. The initial values of the conductivities are taken from the available field pumping test measurements or based on the lithology of individual hydrogeological layers. The vertical conductivities are decreased 10 times in aquifers considering the anisotropic structure of the sedimentary layers. One coefficient per layer is changed during the optimization, i.e. the ratio between the horizontal and vertical conductivity is kept fixed in each optimization run. It is known that the varying anisotropy produces very different flow fields—the flow system is more local with lower anisotropy and more regional with higher anisotropy (Michael and Voss 2009). This effect mainly comes from the differences in conductivities of aquifers and aquitards; still, it is also true for the groundwater flow within the particular aquifer.

The conductivities are assumed uniform throughout a whole individual layer. The exception is Quaternary deposits where the materials of variable conductivities (clay, till, sand, gravel etc.) are mixed in sublayers of variable thickness. In areas with enough borehole data (territory of Latvia) the local horizontal and vertical conductivities are derived from the lithology record of the boreholes. The effective vertical conductivity around each borehole is calculated as a serial sum of the resistances of sub-layers

$$K_{z\_eff} = \frac{\sum_{i=1}^{N} dZ_i}{\sum_{i=1}^{N} \frac{dZ_i}{K_i}}, \quad (6)$$

and the horizontal conductivity as a parallel sum of the resistances of sublayers

$$K_{xy\_eff} = \frac{\sum_{i=1}^{N} dZ_i \cdot K_i}{\sum_{i=1}^{N} dZ_i}, \quad (7)$$

where dZ_i is the thickness and K_i is the conductivity of each sublayer. The values from the boreholes are afterwards extrapolated as constant values within the finite element. The typical conductivity values for the materials are initially set for each of the sublayers. The effective conductivities (horizontal and vertical) are both multiplied by a one variable parameter during the optimization.

 DOI 10.1007/s10040-013-0970-7

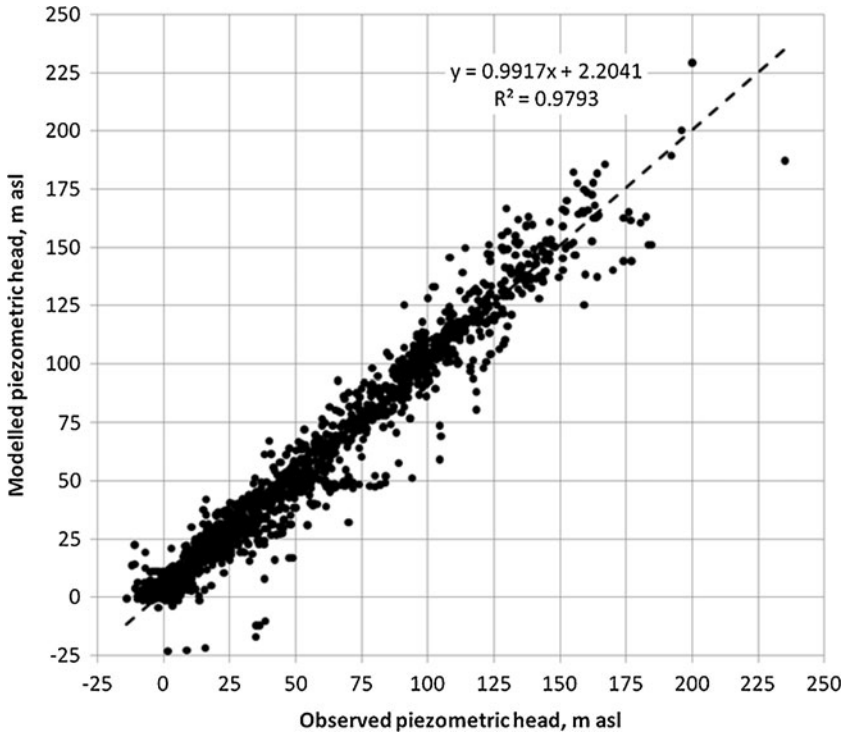

Fig. 5 Modeled piezometric head versus observations. 4,092 observations for the time interval between 1995 and 2005 are plotted. The *dashed line* represents the linear regression

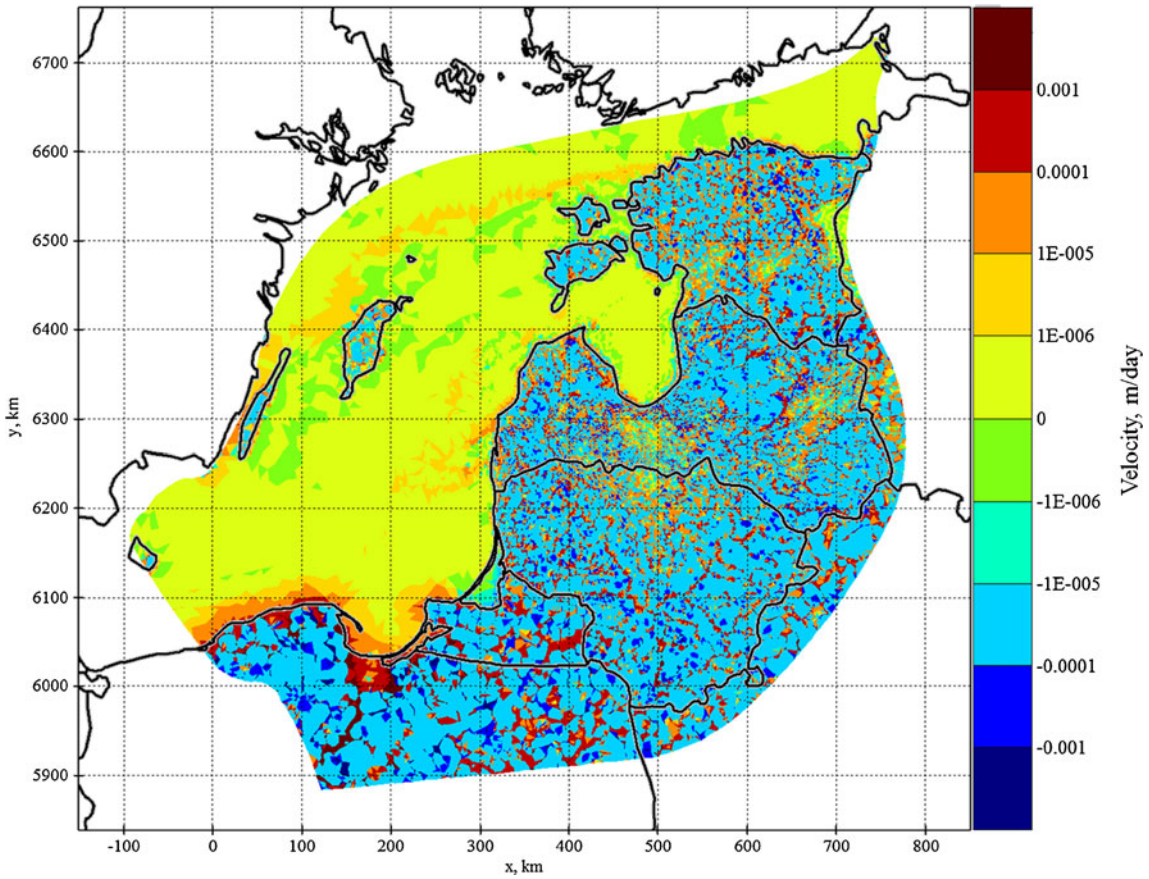

Fig. 6 Vertical velocity [m/day] at the top of the Quaternary layer, in logarithmic scale. *Negative values* represent recharge and *positive values* represent discharge

 DOI 10.1007/s10040-013-0970-7

Figure 3 shows the probability density distribution of the ratio K_{xy}/K_z. There are two pronounced maxima in the distribution—the first at the value slightly larger than 1, which corresponds to nearly uniform lithology in the borehole, and the second to the value around 25, which is the typical ratio in boreholes with non-uniform lithology. There are 25 calibration parameters altogether—one for each of the 24 layers and one for the infiltration rate.

Results

Model calibration

Multi-parameter calibration is performed according to the method described in the previous section "Model calibration using the optimization method". Two calibration stages were performed. The initial values of hydraulic conductivities of the layers for stage 1 were set from the knowledge about the lithology and some manual calibration runs comparing the visual differences between observations and calculations. The initial values for stage 2 were set after analyzing the results of optimization of stage 1. The initial values of hydraulic conductivities for both stages are shown in Table 1. The initial value of infiltration was set to 70 mm/year. The allowed variation range of conductivities for all layers and the infiltration rate is from 0.01 to 100 times of the initial value.

The target function is constructed, according to the method described in the preceding, in 14 layers (Cm, D1-2, D2nr, D2ar-br, D3gj-am, D3pl-dg, D3og-kt, D3st-el, D3fm, C1, P2, T1, J2, Q). Most of the layers are aquifers; however, two thick aquitards D2nr and D3st-el, where enough measurements exist, were also used for the calibration. The target function is normalized so that each layer has the same impact on the summary target function Z. The spatial weighting coefficients (Eq. 2) are constructed with a distance of influence of 1,500 m for all layers. Temporal weighting coefficients (Eq. 3) are constructed using a time of influence of 5 years for layers above D2nr and 40 years in D2nr and deeper.

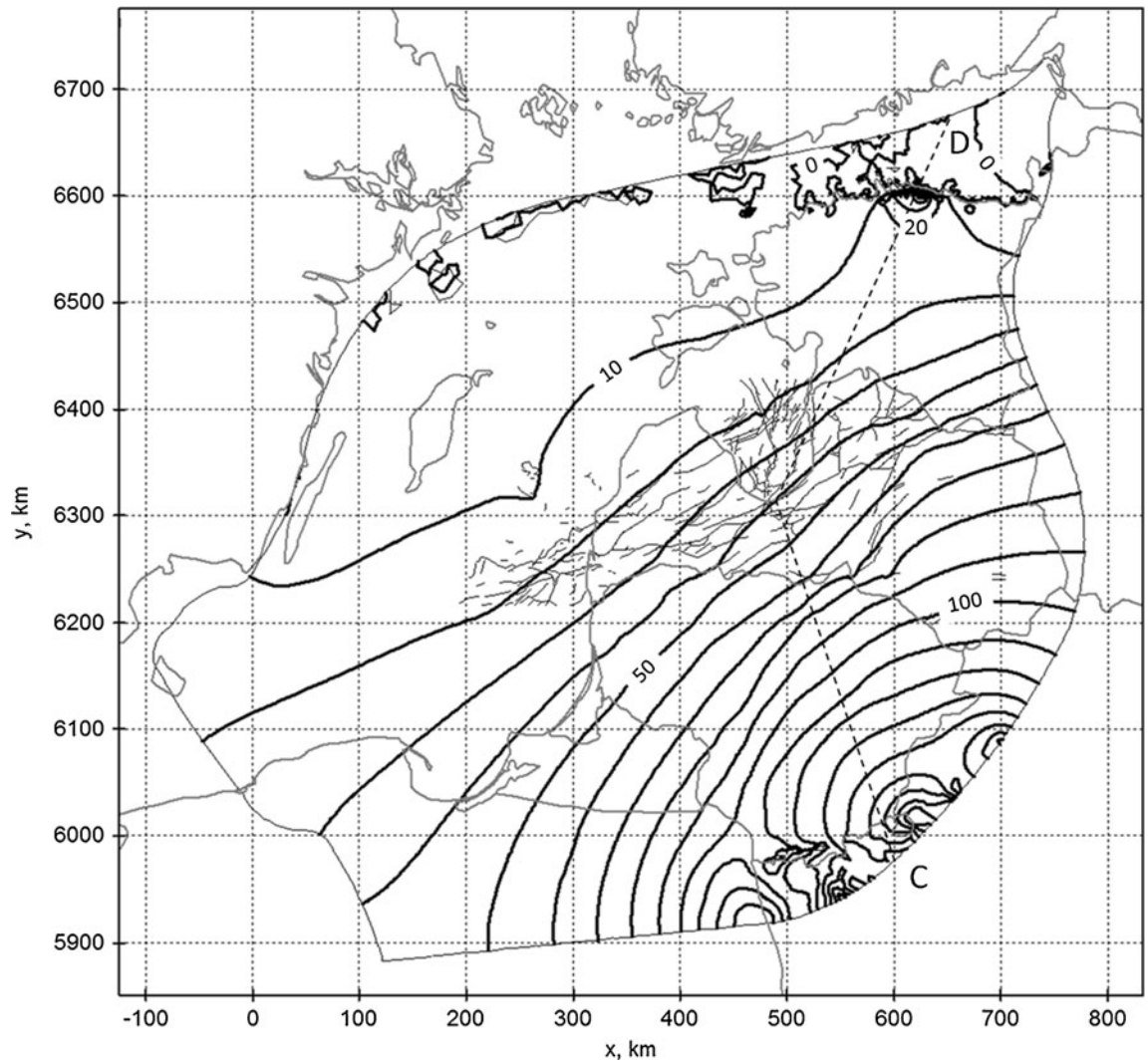

Fig. 7 Piezometric head [m asl] distribution in the Cambrian aquifer

 DOI 10.1007/s10040-013-0970-7

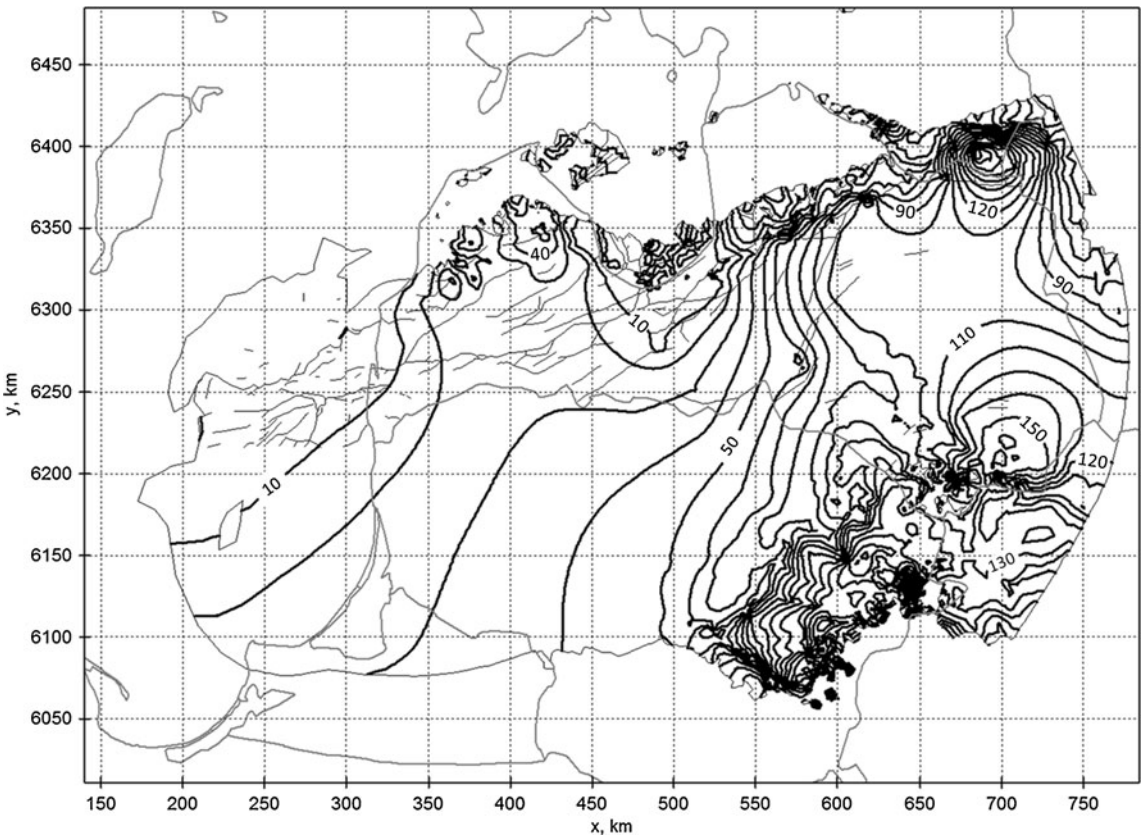

Fig. 8 Piezometric head [m asl] distribution in the upper Devonian Gauja-Amata aquifer

The optimization procedure calculates blocks of 26 iterations slightly changing the parameters, then one iteration with a larger change of parameters is made. The dependence of the target function Z on the iteration is shown in Fig. 4. It can be seen that the solution converges in several hundred iterations. The bold line follows the optimization process starting from the parameter set 1 (see Table 1), the thin line, starting from the parameter set 2 (see Table 1). The employed quasi-Newton optimization method is a gradient-based method and it does not guarantee that the global minimum is found. Therefore, the result is dependent on the initial values of the parameters (hydraulic conductivities) as can be seen in Fig. 4. Dividing the overall target function Z by the number of layers N used in building the target function, and taking the square root, gives the mean RMSE value of 9.0 m (stage 1) and 8.8 m (stage 2), where

$$RMSE = \sqrt{\frac{Z}{N}}. \tag{8}$$

The values of the weighted mean error (WME) and RMSE measures for each layer are used for the estimation of model calibration quality and are shown in Table 2. The $RMSE_j$ value for the layer j is the square root of the target function Z_j and WME_j for layer j is constructed similarly as RMSE using time and spatial weights:

$$WME_j = \frac{1}{\sum_{i=1}^{N} c_{ti} c_r(I_i)} \sum_{i=1}^{N} c_{ti} c_r(I_i)[h_{obs}(t_i, I_i) - h_{mod}(I_i)], \tag{9}$$

see Eq. (4) for explanations.

It can be seen that WME is smaller than +/−5 m for all layers. The RMSE values in the deeper layers Cm and D 1–2 are larger than 10 m but less than 10 m in all other layers, the corresponding relative RMSE value being less than 5 %.

The linear regression was constructed between the target function value and values of parameters to perform the parameter sensitivity tests. All the calculations from stage 1 and stage 2 were included in this regression analysis. The significance test of this regression was applied, determining p-values for each of the parameters (Weisberg, 2005, Kabacoff, 2012). The p-values for the conductivity of each layer are shown in Table 1 and the p-value of infiltration rate is 0.005 (p-values determine the significance of the parameter; a value close to zero is more significant). It can be seen that hydraulic conductivities of all layers are significant parameters within a confidence interval of 0.05 except the aquitards D3og-kt* and D3pl-dg*.

 DOI 10.1007/s10040-013-0970-7

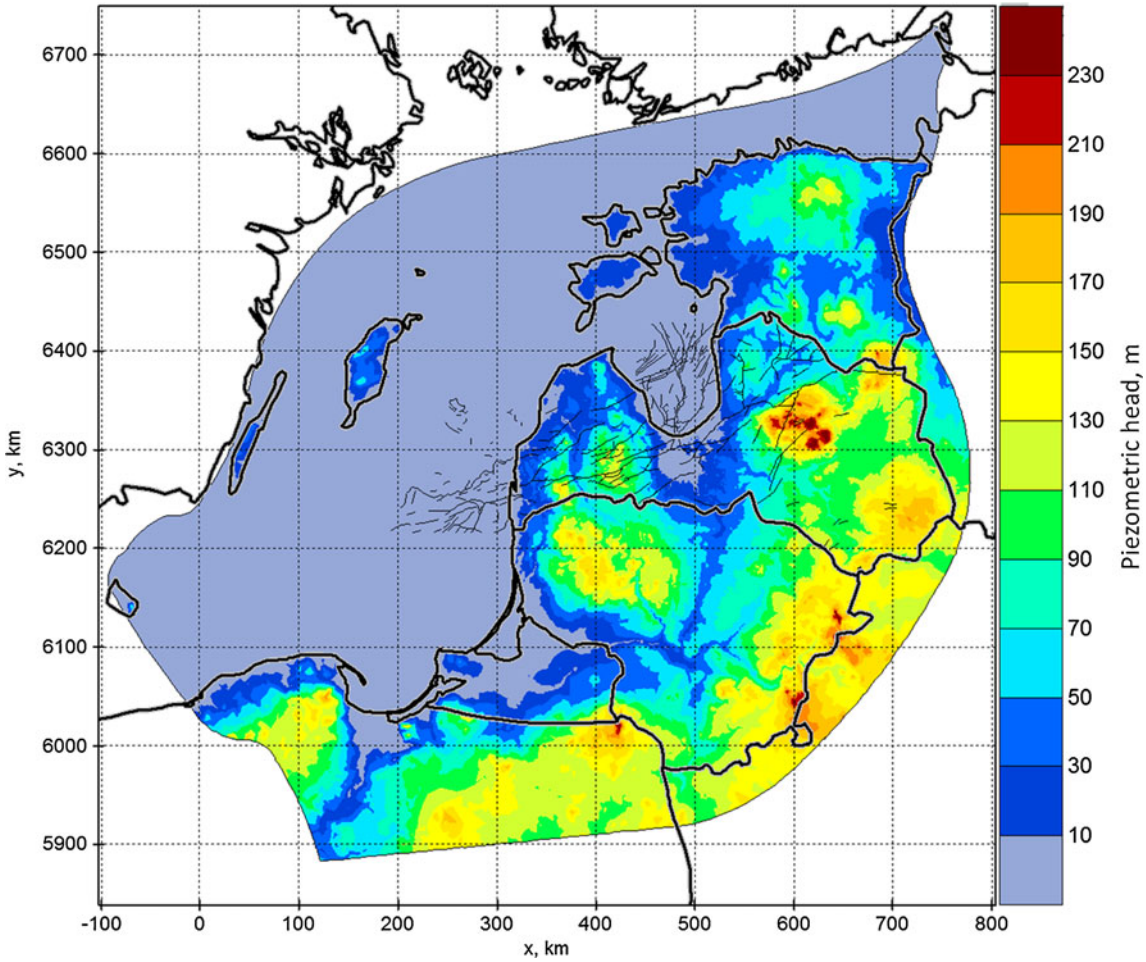

Fig. 9 Piezometric head [m asl] distribution in the Quaternary layer. *Dark lines* are borders of the countries

The sensitivity of the solution on the change of conductivities can be also estimated comparing the results of stage 1 and stage 2. The optimized conductivities in stages 1 and 2 differ by more than one order in many layers (see Table 1) but the resulting RMSE values of both optimization stages are quite close to each other; the maximum difference in one layer is 1.5 m (Table 2). This allows for the conclusion that the target function is not very sensitive to the change of conductivities near the optimum set of calibration parameters. To investigate this behavior in detail, a series of calculations was carried out by varying input parameters one at a time and keeping other parameters constant. Starting from the optimized solution (stage 2) all input parameters were increased and decreased by a small value of ε=0.23 % and the changes of overall target function Z were analyzed. The derivative

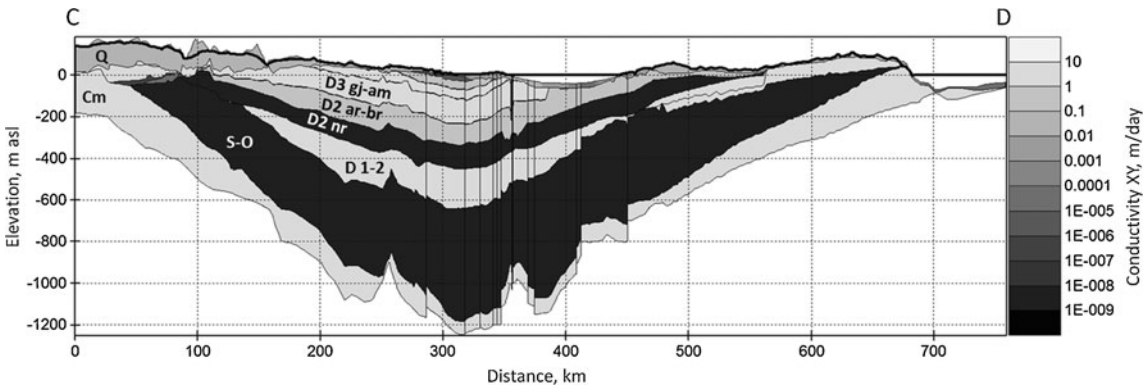

Fig. 10 Hydraulic conductivity K_{xy} [m/day] in the cross-section along the line CD (*dashed line* in Fig. 7)

 DOI 10.1007/s10040-013-0970-7

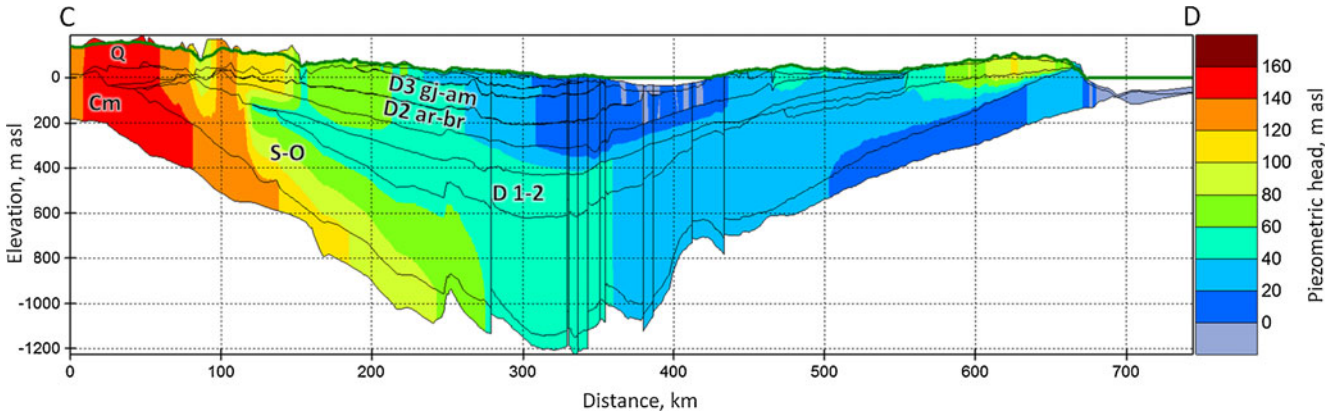

Fig. 11 Piezometric head [m asl] in cross-section along line CD (*dashed line* in Fig. 7). The *bold line* is the level of the water table

of relative target function with respect to the relative change of parameter between cases with largest parameter value ($+\varepsilon$) and smallest parameter value ($-\varepsilon$) is determined as

$$Z_K = \frac{\{Z[K\cdot(1+\varepsilon)] - Z[K\cdot(1-\varepsilon)]\}/Z(K)}{2\varepsilon}, \qquad (10)$$

here K is the hydraulic conductivity of the layer of interest. The derivative Z_K is shown in Table 1. It can be seen that the relative changes of target function are much smaller than the relative changes of conductivities for all layers ($Z_K << 1$). The D3pl-dg, Cm, D3pl-dg*, P2*, D3gj-am and D1-2 layers have the highest relative sensitivity with $Z_K > 2$ %.

In Fig. 5 the modeled piezometric heads for stage 2 are plotted versus observed heads for the time period between year 1995 and 2005, for 4,092 observations. The correlation, with $R^2=0.979$, is very good and comparable with the relative RMSE values. This result can be considered as validation because the calibration is done using time and spatial weights, but in this graph the observations have equal weights for the building of the linear regression line and corresponding R^2 measure. It can be seen that for most of the outlayers the modeled piezometric head value is less than the observed value. Most of them are located in places where the water abstraction is concentrated in one well, when in reality it may be distributed over the administrative district.

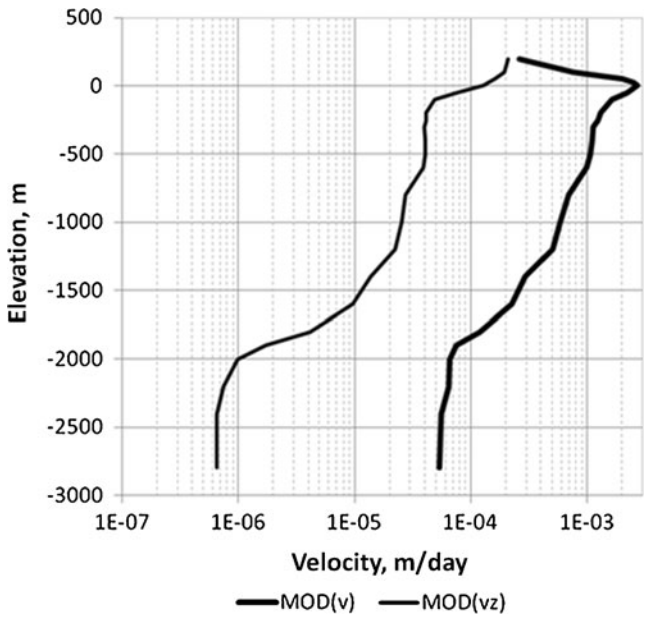

Fig. 12 Modulus of the flow velocity (*bold line*) and vertical flow velocity (*thin line*) as a function of elevation, averaged over horizontal cross-sections

Analysis of the results

Results yielded by calibration stage 2, with the smallest target function, are used for further analysis. Considering the large area of BAB, the results show general flow structures and can not describe any local phenomena. The structure of the groundwater flows in the BAB will be analyzed along and across the layer surfaces as well in the vertical cross-sections.

Figure 6 shows the distribution of vertical velocity of water flow at the top of the Quaternary layer. Negative velocities represent recharge and positive velocities represent discharge. The recharge takes place mainly at high elevations on land. Intensive discharge takes place at low elevations on land (lowlands, valleys of rivers) and slow discharge at the bottom of the Baltic Sea. This distribution is the result of combined fixed head and constant infiltration boundary conditions described earlier.

The flow velocity is proportional to the distance between equipotential lines and to the hydraulic conductivity, which is constant throughout each layer. Equipotential lines of the piezometric head are shown for three layers—Cm (Fig. 7), D3gj-am (Fig. 8) and Q (Fig. 9). In the Cm layer, which represents the groundwater flow in deep aquifers, the recharge area is located in the southeastern part of the BAB where the Cm reaches the Earth's surface coinciding with the

 DOI 10.1007/s10040-013-0970-7

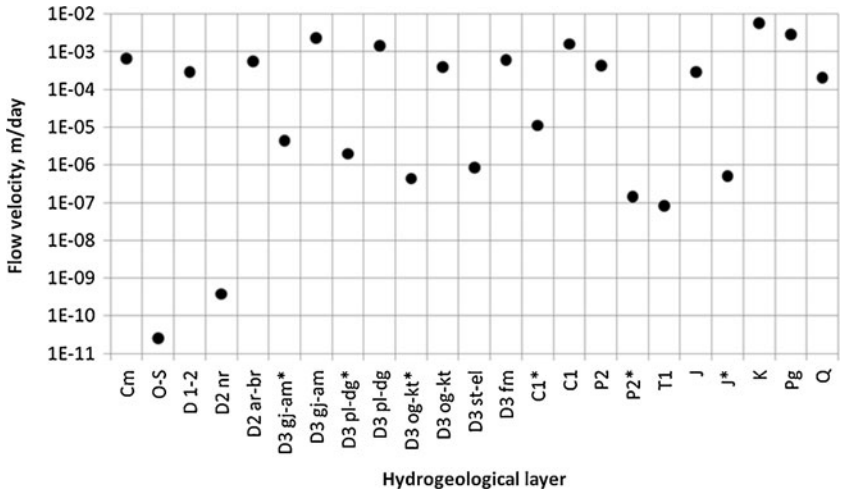

Fig. 13 Average value of modulus of the flow velocity

highest elevations in the surface topography. In the northwest side of the BAB, where the crystalline basement reaches the surface (coast of Sweden and Finland), the Cm layer has a discharge area due to a lower surface elevation compared to the SE side.

In the D3gj-am layer (Fig. 8), which is a constituent of the upper active exchange zone according to Levins et al. (1998), the general flow structure is similar—recharge in the higher eastern part and discharge in the lower western part. However, in this layer more local features are present as a discharge area in the Gulf of Riga where water flows from both the east and the west (Fig. 8). High local gradients are present in the northern and southeastern parts of the D3gj-am layer, where it reaches the sub-Quaternary surface. Discharge is also present in valleys of rivers Gauja (north) and Daugava (east) where the D3gj-am reaches the earth's surface. In the Quaternary layer (Fig. 9), the distribution of piezometric head follows the topography very well and many local features, present in topography, are also represented in the head distribution.

The conductivity in the xy direction, derived from the automatic calibration, is shown in the vertical section along the line CD (see Fig. 7) in Fig. 10. Two noticeable aquitards, O-S and D2nr, divide the BAB into three parts (flow systems) which are relatively well isolated from each other, attesting to the general perception of the groundwater flow in the BAB as described by Mokrik (1997). The deepest part is the Cm layer, which provides transit flow from the southeastern to the northwestern side of the BAB and is well isolated from other layers by the Silurian-Ordovician aquitard in most areas. The groundwater flow in the lower Devonian D1-2 layer also has a transit character and is directed from SE to NW. The middle and upper Devonian aquifers are divided by several thin aquitards. This division is based on the piezometric head observations, suggesting that the groundwater flow has some disconnections in these aquifers, while a detailed lithological composition in this particular formation is usually omitted in the lithological descriptions of the boreholes used in the construction of the geometric model. The distribution of piezometric heads in the same cross-section is shown in Fig. 11. It can be seen that the main recharge area with a high head is on the left side of the section (southeast, point C), whilst the discharge areas are in the Gulf of Riga (mid-section) and in the north of the BAB. The flow structure in the upper aquifers has a more local character.

Faults are regarded as a surface along which sediments are vertically displaced in the model, e.g., the groundwater flow in the Eidiacaran (Vendian)-Cambrian (Cm) aquifer is partly disconnected along the Pleskava–Liepāja fault line. In terms of the pressure head, there is no major disruption along the faults. This situation is explained through the model setup: even though faults disconnect the groundwater flow in the Cm layer, the fact that this layer is recharged and discharged so far apart (southern Lithuania and northern Estonia) means that the vertical flow has much larger influence on the pressure head distribution than the horizontal flow in the aquifer. The maximal jump in the pressure head observed in the model is approximately 10 m (along the fault in northeastern Latvia and southern Estonia), which is in the range of calculated head precision.

Principal flows and integral parameters

The computed groundwater flow of the BAB allows one to carry out the analysis of the flow budget between the layers and to compute the integral parameters. The total volume of the sedimentary rocks within the BAB is 579,000 km^3, where O-S (42 %) and Cm (12 %) are the sediments that constitute the largest part by volume. The mean groundwater flow velocity over the whole BAB is 2.9e-4 m/day and its direction is 333° (from southeast to northwest). The

 DOI 10.1007/s10040-013-0970-7

mean value of the velocity modulus over the whole BAB is 8.2e-4 m/day.

The mean flow velocity as a function of depth is analyzed in Fig. 12. The bold line represents the mean value of the velocity modulus, the thin line represents the mean value of the modulus of the vertical velocity component. The vertical velocity is dominant in aquitards with low conductivity, whereas the flow is mainly horizontal in aquifers. In all aquifers the mean horizontal velocity component is at least 20 times higher than the vertical velocity component, whereas in most aquitards the vertical component is 10 or even 100 times higher (exceptions are thick aquitards C1*, P2*, J*). At high elevations, where the recharge takes place, the flow velocity has the highest vertical component of 0.2 mm/day. With depth the vertical velocity decreases, down to 1 μm/day at depths of 2 km. The velocity modulus (i.e. the horizontal flow component) has a maximum mean value of 2 mm/day at sea level and decreases to 0.05 mm/day at the deepest levels. The maxima at sea level may be explained by many local recharges and discharges in the Quaternary layer. The modulus of the flow velocity decreases with depth only by one order of magnitude, while the modulus of the vertical velocity decreases by two orders of magnitude. This result proves the existence of a significant transit flow in the Cambrian layer which is separated from the rest of the flow system.

Figure 13 shows the mean values of velocity moduli in all layers of the BAB. The thick aquitards O-S and D2nr show by far the lowest flow velocities, under 10^{-9} m/day. The highest mean velocities, over 10^{-3} m/day, are in layers Cm, D3gj-am, D3pl-dg, C1, K and Pg. In other aquifers, velocities are between 10^{-4} and 10^{-3} m/day and, in other aquitards, the flow velocities are between 10^{-9} and 10^{-5} m/day. This analysis concludes that the deeper aquifers are not excluded from the water exchange in the BAB because the flow velocities are similar to those in higher aquifers. This results from the structure of the BAB where almost all aquifers have partial contact with the sub-Quaternary surface. The water in the central parts of the deeper aquifers can be older because the main groundwater flow comes from the recharge areas at the margins of the BAB. However, assuming steady-state conditions, no dispersion, porosity of 0.2 and a typical flow velocity of 10^{-3} m/day in aquifers, the distance accomplished during the Holocene (last 10,000 years), assuming constant groundwater flow directions and piezometric heads, is 13.25 km. This distance is small compared to the size of any aquifer; therefore, it is not possible to conclude that water is older in deeper aquifers from a steady-state model.

Integrating the flow through the boundaries between individual layers allows the calculation and analysis of the water balance. The integrals of inflowing and outgoing flows through each surface are built. The total recharge through the earth (and sea) surface is 2.63e7 m^3/day, the discharge is 2.61e7 m^3/day and the water abstraction is 2.5e5 m^3/day. The imbalance of these numbers signifies a numerical error and the value of the imbalance constitutes 0.08 % of the recharge value. The water abstraction is 1 % of the total recharge in BAB; however, this ratio should be considered in context, i.e. that the recharge does not include the sub-mesh scale flows (section "Hydrogeological model") and not all wells are included in the model. Taking together all Devonian layers, the total inflow through the boundary is 4.9e6 m^3/day, the outflow is 4.7e6 m^3/day and the water abstraction is 3 %. In Cm, the deepest aquifer, the inflow and outflow integrals are 6.2e5 m^3/day.

Groundwater flow in the Baltic coastal area in the upper, active water exchange zone is directed from the land into the Baltic Sea, and, according to the results of this study, discharge occurs mainly in the coastal area. The total discharge flowing through the vertical plane into the Baltic Sea is 3.5e6 m^3/day. 96 % of the total discharge flows through aquifer K (61 %), Q (30 %) and Cm (5 %). The effect of these three layers can be seen in Fig. 6 as intensive discharge near the coastline (Q), near the Polish coast (K) and in the NW part of the Baltic Sea, where the aquifer Cm reaches the sub-Quaternary surface. The discharge to the sea is 14 % of the total recharge, taking place on the land. The model does not show any remarkable evidence of seawater recharge into the aquifer system.

Part of the groundwater system in the BAB is artesian, i.e. the piezometric head is higher than the surface elevation of the corresponding layer. The calculation results allow for extracting the volume of the BAB where the artesian head is positive. This integral analysis shows that, for most aquifers containing drinking water (D2ar-br and higher), the part with positive artesian head is between 19 and 24 %, except for D3og-kt with 15 %, C1 with 33 % and K with 7 %.

Conclusions

The geometric model, built using heterogeneous data sources and newly developed algorithms, resulted in geometry and a FE mesh, which allowed achievement of good calibration results. This was achieved despite the crude assumption of uniform material properties for each layer across the whole area of the BAB. The results of the hydrogeological model of the BAB demonstrate that generally the flow is directed from southeast to northwest, but the local topography shows a strong influence on the shallower aquifers. The discharge to the sea is 14 % and the water abstraction is 2 % of the total recharge. There is an intensive transit flow in the Cm aquifer system. This flow is separated from upper layers by the thick aquitard O-S. In about 25 % of the aquifers' volume, the artesian head is positive.

Acknowledgements The present work has been funded by the European Social Fund project "Establishment of an interdisciplinary scientist group and modelling system for groundwater research" (Project No. 2009/0212/1DP/1.1.1.2.0/09/APIA/VIAA/060).

 DOI 10.1007/s10040-013-0970-7

Appendix

Comparison with analytical solution

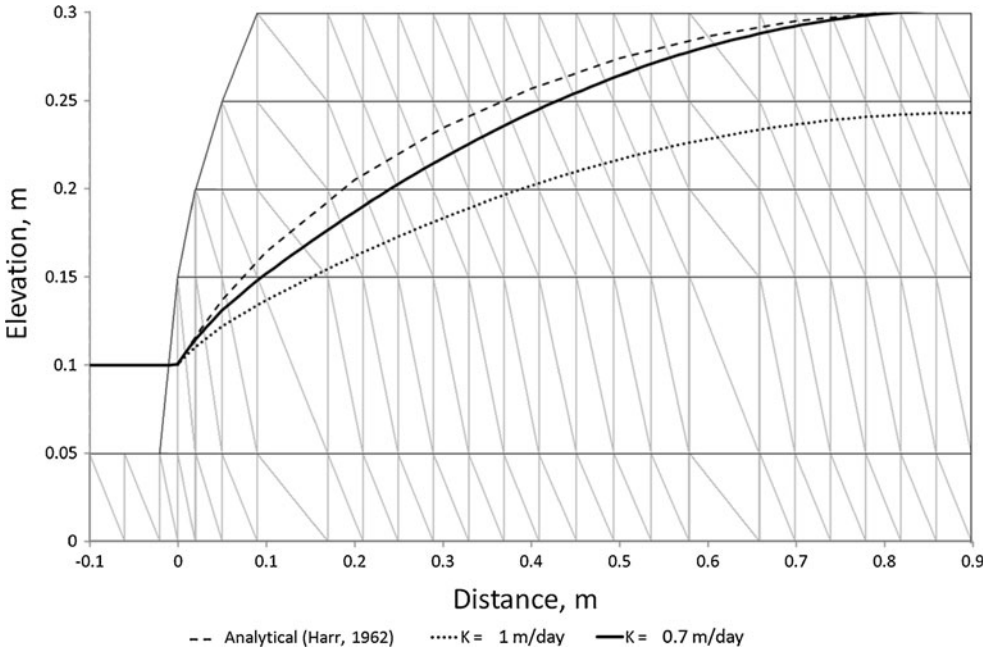

Fig. 14 Groundwater level between reservoirs. *Dashed line*: analytical solution (Harr 1962); *dotted line*: MOSYS solution (K=1 m/day); *solid line*: MOSYS solution (K=0.71 m/day), *gray lines*: FE mesh

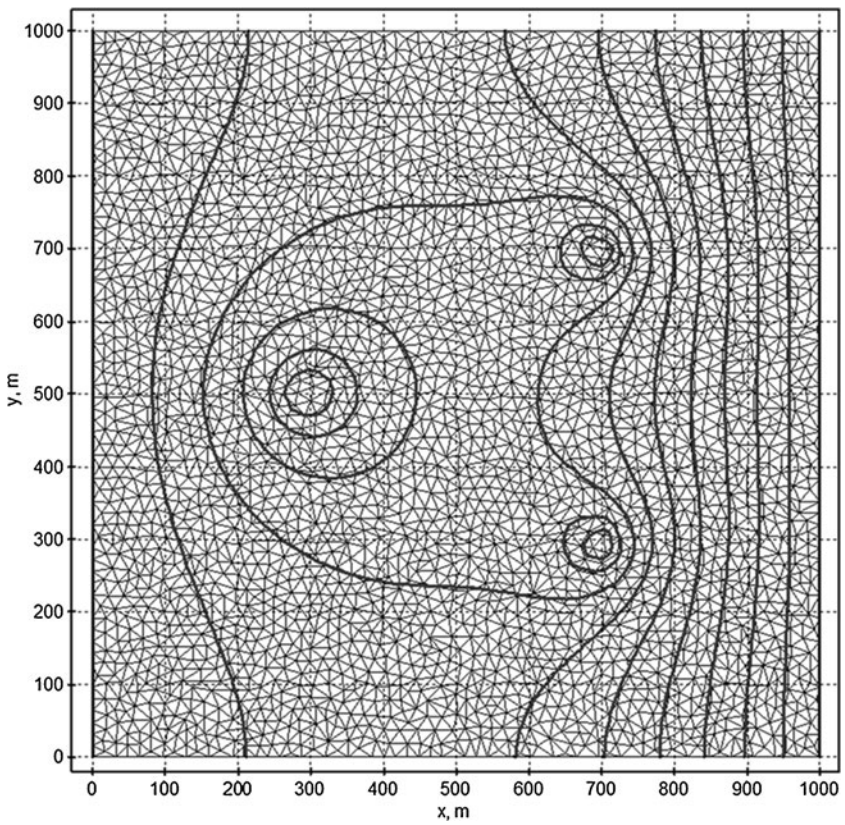

Fig. 15 Triangular mesh and isolines of piezometric head with step of 0.1 m. Head h=0.5 m at x=0 m and h=1 m at x=1,000 m

 DOI 10.1007/s10040-013-0970-7

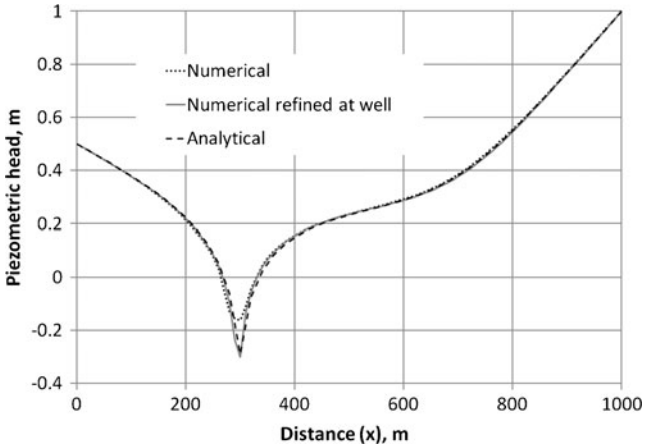

Fig. 16 Analytic solution (*dashed line*) and numerical results (*dotted line*; and *solid gray line* for the refined solution) at y=500 m

The model is validated against solutions of analytic problems. The first comparison is carried out with the analytical solution of the groundwater flow between two water reservoirs with fixed levels and uniform infiltration between them (Harr 1962). The analytical solution for the water level is predicted as

$$h^2 = h_0^2 - \frac{\left(h_0^2 - h_L^2\right)x}{L} + \frac{W}{K_S}(L-x)x, \tag{11}$$

where h is the water level, x is the position between the reservoirs, W is the recharge rate in m/s, K is the hydraulic conductivity in m/s, h_0 and h_L are the water levels at x=0 and x=L, respectively. Both water levels are equal and only half of the domain is modeled because the solution in this case is symmetric to the vertical line x=L/2. The length of the domain for the analytic solution (L) is 1.8m, h_0=h_L=0.1m, W=0.1m/day and K=1m/day. The numeric domain starts at x=−0.1m and ends at x=1m, the water head is set as a boundary condition h(−0.1–0)=0.1m, and the recharge rate W(0–0.91)=0.1m/day. In Fig.14, the analytical (dashed line) and numerical (dotted line for K=1m/day and solid line for K=0.71m/day) solutions are shown in vertical cross-section with the numerical FE mesh as gray lines in the background.

The analytical solution shows a slightly higher piezometric head distribution than the modeling results using the same conductivity, K=1m/day. This is expected due to the simplified treatment of the unconfined zones—in the model the water can also flow through the elements above the water table. If the conductivity in the numerical solution is decreased so that the maximum values of the piezometric head are equal (at K=0.71m/day), the numerical solution is closer to the analytical one (solid line in Fig.14). As the conductivity values in the BAB are not exactly known and will be calibrated anyway, the agreement with the analytical solution is acceptable for the practical application.

The other case for comparison relates to the analytical solution in the confined multi-well aquifer. The analytical solution for the head change h' caused by pumping wells is given in Yeo and Lee (2003):

$$h'(x,y) = \frac{-4}{\pi^2}\sum_{m=1}^{\infty}\sum_{n=1}^{\infty}\frac{\sum_{i=1}^{p} q_i \sin\frac{n\pi x_i}{L}\sin\frac{m\pi y_i}{H}}{\left(T_x n^2 \frac{H}{L} + T_y m^2 \frac{L}{H}\right)}\sin\frac{n\pi x}{L} \times \sin\frac{m\pi y}{H}, \tag{12}$$

where L is the domain size along the x axis, H is the domain size along the y axis, T_x and T_y are the hydraulic transmissivities in the x and y directions, respectively, x_i and y_i are the co-ordinates of the pumping wells, p is the number of wells, q_i is the pumping rate of the i-th well.

Three wells with a pumping rate of 1m^3/day are positioned at (x,y)=(300, 500), (700, 300), (700, 700). The head is fixed to h=0.5m at x=0m and to h=1m at x=1,000m. No-flow boundaries are set at y=0m and y=1,000m. In the analytical solution, this boundary condition is realized extending the domain in the y-direction 5 times and using 12 imaginary wells, similar to the situation described in Yeo and Lee (2003). The thickness of the aquifer is 1m and conductivity K_x=K_y=K_z=1m/day, resulting in T_x=T_y=1m^2/day for the analytical solution. The mesh size is uniform with a target triangle area of 250m^2. The triangle mesh (thin lines) and isolines of the piezometric head distribution (bold lines) are shown in Fig.15. The comparison of the analytical (dashed line) and numerical (dotted line) solutions along line y=500m in Fig.16 shows a good agreement between both. The differences in elements near the well can be reduced by local grid refinement (gray solid line), where the target triangle area is 50m^2 within a radius of 50m from the first well.

References

Bastani M, Kholghi M, Rakhshandehroo GR (2010) Inverse modeling of variable-density groundwater flow in a semi-arid area in Iran using a genetic algorithm. Hydrogeol J 18:1191–1203

Brangulis AP (1985) Vendian and Cambrian of Latvia. Zinatne, Riga

Brangulis AJ, Kaņevs S (2002) Latvijas tektonika [Tectonics of Latvia. State Geological Survey, Riga

Brangulis AJ, Kurss V, Misans J, Stinkulis G (1998) Geology of Latvia. Geological map of 1:500 000 scale and description of the PreQuaternary deposits (in Latvian). State Geological Survey, Rīga

Carrera J, Alcolea A, Medina A, Hidalgo J, Slooten LJ (2005) Inverse problem in hydrogeology. Hydrogeol J 13(1):206–222

Cherubini C, Pastore N (2011) Critical stress scenarios for a coastal aquifer in southeastern Italy Nat Hazards Earth Syst Sci 11(1381–1393):2011. doi:10.5194/nhess-11-1381-2011

Folch, Mas-Pla (2008) Hydrogeological interactions between fault zones and alluvial aquifers in regional flow systems. Hydrol Process 22(17):3476–3487

DOI 10.1007/s10040-013-0970-7

Foley MG (1994) West Siberian basin hydrogeology: regional framework for contaminant migration from injected wastes. International Symposium on the Scientific and Engineering Aspects of Deep Injection Disposal of Hazardous and Industrial Wastes, Berkeley, CA, May 1994

Harr ME (1962) Groundwater and seepage. McGraw-Hill, New York

Harrar WG, Sonnenborg TO, Henriksen HJ (2003) Capture zone, travel time, and solute-transport predictions using inverse modeling and different geological models. Hydrogeol J 11:536–548

Jarvis A, Reuter HI, Nelson A, Guevara E (2008) Hole-filled SRTM for the globe, version 4. Available from the CGIAR-CSI SRTM 90m database. http://www.cgiar-csi.org/data/srtm-90m-digital-elevation-database-v4-1. Accessed 6 Feb 2013

Juodkazis VI, Paltanavicitjs JP (1976) Filtration properties of slightly conductive layers of the Baltic artesian basin and methods of their investigation. Proceedings of the symposium Hydrogeology of Great Sedimentary Basins, IAHS/Hungarian Geological Institute, Budapest, May–June 1976

Juodkazis V (1982) PreQuaternary sediment hydrogeological map of the Baltic republics USSR Ministry of Geology, LitNIGRI, Vilnius, Lithuania, 84 pp (in Russian)

Kabacoff RI (2012) Quick-R. http://www.statmethods.net/stats/regression.html. Accessed 29 September 2012

Kovalevskij MI, Ozolins NK (1967) Tectonic structure of the Eastern European platform western block (in Russian). In: Questions of the Middle and Upper Paleozoic geology in Baltics. Zinatne, Riga

Levins I, Levina N, Gavena I (1998) Latvian groundwater resources. State Geological Survey, Riga

Malolepszy Z (2005) Three-dimensional geological model of Poland and its application to geothermal resource assessment. Workshop Geological Models for Groundwater Flow Modeling, Extended Abstracts, October 2005, Annual Meeting, Geological Society of America, Salt Lake City, UT

McDonald MG, Harbaugh AW (1989) A modular three-dimensional finite-difference ground-water flow model. US Geol Surv Open File Rep 83–875

Michael HA, Voss CI (2009) Controls on groundwater flow in the Bengal Basin of India and Bangladesh: regional modeling analysis. Hydrogeol J 17:1561–1577

Mokrik R (1997) The paleohydrogeology of the Baltic Basin: Vendian and Cambrian. Tartu University Press, Tartu, Estonia

Nocedal J (1980) Updating quasi-Newton matrices with limited storage. Math Comput 35:773–782

Normani SD, Sykes JF (2012) Paleohydrogeologic simulations of Laurentide ice-sheet history on groundwater at the eastern flank of the Michigan Basin. Geofluids 12:97–122

Paczynski B, Jezierski H, Mitrega J, Plochniewski Z, Skrypczyk L, Wodzinska I (1993) Hydrogeological atlas of Poland, scale 1:500,000, part I: fresh groundwater aquifer systems. Panstwowy Instytut Geologiczny, Warsaw, 24 pp, 4 maps

Ravazzani G, Rametta D, Mancini M (2011) Macroscopic cellular automata for groundwater modelling: a first approach. Environ Model Software 26:634–643

Schenk O, Gartner K (2006) On fast factorization pivoting methods for symmetric indefinite systems. Elec Trans Numer Anal 23:158–179

Spalvins A, Janbickis R, Slangens J, Gosk E, Lace I, Viksne Z, Atruskievics J, Levina N, Tolstovs J (1996) Hydrogeological model "Large Riga" (in Latvian and English). Atlas of map. Riga Technical University, Riga; State Geological Survey of Latvia, Riga; Geological Survey of Denmark and Greenland, Copenhagen, 102 pp

Spalvins A, Slangers J, Lace I, Stuopis A, Domasevicius A (2009) Creating a regional hydrogeological model for south-east of Lithuania. (Scientific journal of Riga Technical University) Comput Sci 41:13–20

SciPy community (2011) SciPy Reference Guide, Release 0.10.0.dev. http://docs.scipy.org/doc/scipy/scipy-ref.pdf. Accessed 15 September 2011

Seifert T, Tauber F, Kayser B (2001) A high resolution spherical grid topography of the Baltic Sea, 2nd edn. Proceedings of the Baltic Sea Science Congress, Stockholm, 25–29 November 2001. http://www.io-warnemuende.de/topography-of-the-baltic-sea.html. Accessed 03 February 2012

Sorokin SV, Larskaya LA, Savvaitova LM (1981) Devonian and carbon of the Baltics Zinatne, Riga (in Russian)

Stuopis A, Gregorauskas M, Domasevicius A (2010) Formation of groundwater runoff in Nemunas RBD (Lithuania). (Scientific journal of Riga Technical University) Comput Sci 45:16–26

Takčidi E (1999) Datu bāzes "Urbumi" dokumentācija [Documentation of the database "boreholes"]. State Geological Survey, Riga

Trefry MG, Muffels C (2007) FEFLOW: a finite-element ground water flow and transport modeling tool. Ground Water 45(5):525–528

Tuulig I, Floden T (2009) Seismic correlation of Paleozoic rocks across the northern Baltic Proper: Swedish–Estonian project since 1990, a review. Estonian J Earth Sci 58(4):273–285

Ulste R (1961) Ordovician. In: Danilans I, Liepins P, Springis K (eds) Geology of the Latvia SSR (in Latvian). Zinatnu akademijas izdevnieciba, Riga, pp 40–47

Usaityte D (2000) The geology of the southeastern Baltic Sea: a review. Earth Sci Rev 50:137–225

Vallner L (2003) Hydrogeological model of Estonia and its applications. Proc Estonian Acad Sci Geol 52(3):179–192

Vetrennikovs V (1996) Tectonic map of the Latvia and the Baltic Sea chrystalline basement in scale 1:1 000 000 (in Latvian). State Geological Survey, Riga

Weisberg S (2005) Applied linear regression. Wiley, Chichester, UK

Welsh WD (2006) Great Artesian Basin transient groundwater model. Bureau of Rural Sciences, Canberra. http://adl.brs.gov.au/brsShop/data/gabtransient1.pdf. Accessed 10 Mar 2011

Welsh WD, Doherty J (2005) Great Artesian Basin groundwater modelling. Engineers Australia, 29th Hydrology and Water Resources Symposium, Canberra, Australia, February 2005

Zienkiewicz OC, Taylor RL (2000) The finite element method, 5th edn, vol 1: the basis. Butterworth-Heinemann, Oxford

Zuzevicius A (2010) The groundwater dynamics in the southern part of the Baltic Artesian Basin during the late Pleistocene. Baltica 23(I):1–12

Yeo IW, Lee K (2003) Analytical solution for arbitrarily located multiwells in an anisotropic homogeneous confined aquifer. Water Resour Res 39(5):1133

 DOI 10.1007/s10040-013-0970-7